

Cementation of Sand Soil by Microbially Induced Calcite Precipitation at Various Degrees of Saturation

Liang Cheng¹, Ralf Cord-Ruwisch², Mohamed A. Shahin³

¹Liang CHENG: Ph.D. student, School of Biological Sciences and Biotechnology, Murdoch University, South Street, Murdoch, Western Australia, 6150, Australia. Email: L.Cheng@murdoch.edu.au

²Ralf Cord-Ruwisch: Senior Lecturer, School of Biological Sciences and Biotechnology, Murdoch University, South Street, Murdoch, Western Australia, 6150, Australia. Email: R.Cord-Ruwisch@murdoch.edu.au

³Mohamed A. Shahin: Associate Professor, Department of Civil Engineering, Curtin University, Perth WA, 6845, Australia. Email: M.Shahin@curtin.edu.au

Corresponding author: Liang CHENG: Ph.D. student, School of Biological Sciences and Biotechnology, south street campus, Murdoch University, 90 South Street, Murdoch, Western Australia, 6150, Australia. Email: L.Cheng@murdoch.edu.au & c_howking@hotmail.com Tel: +61-8-93602403; Fax: +61-8-93107084;

Submitted to: **Canadian Geotechnical Journal**

1 **Cementation of Sand Soil by Microbially Induced Calcite** 2 **Precipitation at Various Saturation Degrees**

3 **Liang Cheng, Ralf Cord-Ruwisch, Mohamed A. Shahin**

4 **Abstract:**

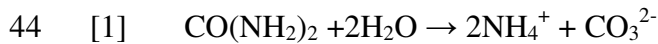
5 A newly emerging microbiological soil stabilization method, known as microbially
6 induced calcite precipitation (MICP), is tested for geotechnical engineering
7 applications. MICP is a promising technique that utilizes the metabolic pathways of
8 bacteria to form calcite precipitation throughout the soil matrix, leading to an increase
9 in soil strength and stiffness. This paper investigates the geotechnical properties of a
10 sand bio-cemented under different degrees of saturation. A series of laboratory
11 experiments was conducted, including sieve analysis, permeability, unconfined
12 compressive strength, consolidated undrained triaxial, and durability tests. The results
13 indicate that higher soil strength can be obtained at similar CaCO_3 content when the
14 treatment is performed under low degree of saturation. Fine sand samples exhibited
15 higher cohesion but lower friction angle than coarse sand samples with similar CaCO_3
16 content. The results also confirm the potential of MICP as a viable alternative technique
17 for soil improvement in many geotechnical engineering applications, including
18 liquefiable sand deposits, slope stabilization and subgrade reinforcement. The freeze
19 thaw and acid rain resistance of MICP treated sand has also been tested.

20 CE Database keywords: Soil stabilization; Cementation; Microorganisms; Calcium
21 carbonate; Durability.

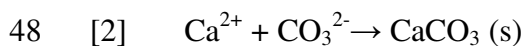
22 1 Introduction

23 Current soil improvement applications include soil replacement, preloading for
24 achieving consolidation, chemical admixture and grouting stabilization. These
25 techniques are time consuming, expensive and in the case of grouting and admixture
26 stabilization are environmentally detrimental (DeJong et al. 2010). In 1974 in Japan a
27 case study documented by Karol (2003) illustrated the environmental impact when
28 acrylamide grout leached into waterways causing five substantiated cases of water
29 poisoning. As a result a ban was placed on nearly all chemical grouts, further
30 reverberating to other countries to apply similar prohibition (Karol 2003). Therefore,
31 continuing studies into finding alternative soil improvement methods are vital to
32 achieve optimum performance, economic viability and environmental sustainability.

33 Calcite *in-situ* precipitation system (CIPS) and microbially induced calcite precipitation
34 (MICP) have been the subjects of research for several industrial applications.
35 Improvement of soil mechanical properties by MICP is currently of particular interest to
36 engineers and microbiologists, and has been demonstrated by several researchers at
37 varying scales (DeJong et al. 2006; Whiffin et al. 2007; van Paassen et al. 2010). The
38 technique can alter the soil characteristics to increase the shear strength and stiffness,
39 while maintaining adequate permeability (Burbank et al. 2011). The technique involves
40 introducing aerobically cultivated bacteria with highly active urease enzyme into soil,
41 harnessing the urease enzyme to catalyze the hydrolysis of urea to produce ammonium
42 and carbonate ions. The chemical reaction involved in this process is shown as follows
43 (Eq. 1):



45 In the presence of an introduced calcium source, often calcium chloride (CaCl_2), the
46 calcium carbonate (CaCO_3 , calcite) forms throughout the soil matrix based on the
47 following chemical reaction (Eq. 2):



49 The produced microbially induced CaCO_3 precipitates bridge adjacent soil particles by
50 cementing the soil grains together to form cemented sand illustrative of calcareous rock
51 (DeJong et al. 2006).

52 Controlling the MICP process and predicting the resulting material properties are
53 essential in improving the engineering properties of porous solid materials (e.g. soil).
54 Many researchers have investigated the empirical correlations between the amount of
55 precipitated CaCO_3 crystals and soil engineering parameters such as the soil porosity,
56 strength, stiffness and permeability (Ismail et al. 2002a, 2002b; Whiffin et al. 2007).
57 The initial properties of soils and the precipitated CaCO_3 crystals can vary in mineral
58 type, density, shape, size distribution and texture (Mitchell and Ferris 2006; Ismail et al.
59 2002a; Warren et al. 2001), which might give an explanation for the observed
60 differences in the resulting engineering properties of MICP treated soils.

61 In a previous study carried out by Cheng and Cord-Ruwisch (2012), more effective
62 crystals precipitating at the sand particles contact points were achieved under a low
63 degree of saturation. This suggested that by controlling the *in-situ* saturation conditions
64 during the MICP process, the distribution of crystals can be predominantly controlled

65 and restricted to the inter-particle contact points. In the current paper, the feasibility of
66 MICP as a promising ground improvement technique is evaluated via a series of
67 laboratory tests using sand columns under various saturation conditions. The laboratory
68 results demonstrate the potential of this technique for geotechnical engineering
69 applications such as preventing liquefaction and improving the stability of
70 embankments.

71 **2 Materials and Testing Methods**

72 **2.1 Sand Soil Tested**

73 Two different types of pure silica sand (Cook Industrial, Minerals Pty. Ltd. Western
74 Australia) were selected for the current study. Sieve analysis was performed for both
75 fine and coarse grained sands to determine the particle size distribution, which is one of
76 the primary components that govern the mechanical behavior of soils. The particle size
77 distribution curves of the fine and coarse sands used are shown in Figure 1. Both sands
78 are classified as poorly graded sand according to the Unified Soil Classification System
79 (USCS). Poorly graded sands were selected as they exhibit undesirable engineering
80 behavior for most geotechnical engineering applications. Both sands have a specific
81 gravity of 2.62.

82 **2.2 Bacterial Suspension and Cementation Solution for MICP System**

83 The urease active strain of *Bacillus sphaericus* (MCP-11) (DSM 23526, available now
84 from DSMZ, Germany), which was isolated from the previous study (AI-Thawadi and
85 Cord-Ruwisch 2012), was used in the current experiments. The isolated strain (MCP11)
86 was cultivated under sterile aerobic batch condition in yeast extract based medium (20

87 g/L yeast extract, 0.17 M ammonium sulphate, 0.1 mM NiCl₂•6H₂O, pH 9.25). After 24
88 hours incubation at 28°C, the culture was harvested and stored at 4°C prior to use. The
89 optical density (OD₆₀₀) of the harvested bacterial suspension varied between 1.5 to 2.0,
90 and the urease activity was approximately 10 U/ml (1 U = 1 μmol urea hydrolyzed per
91 min). The CaCO₃ precipitation rate, depending on the amount of urease activity
92 introduced, can affect the size of the crystals and in turn the bonding force of the CaCO₃
93 crystal bridges and corresponding strength of the treated soil (Ismail et al. 2002a). In
94 this study, the average CaCO₃ precipitation rate was about 10 g/L (solution)/h. The
95 cementation solution consisted of 1 M urea and 1 M CaCl₂.

96 2.3 Sample Preparation

97 The sample preparation started with packing the dry sand (fine and coarse) into a PVC
98 column of 160 mm in height and 55 mm inner diameter. The final dry density and
99 porosity of the sand samples were about 1.62-1.63 g/cm³ and 39%, respectively.
100 Various amounts of water were then flushed from top to bottom to provide the desired
101 degree of saturation within the sand matrix. The degree of saturation is the volume of
102 water in the voids, expressed as percentage of the total volume of voids, according the
103 following equation (Eq. 3):

104 [3] Saturation Degree, $S(\%) = \frac{V_{water}}{V_{voids}} \times 100$

105 where; V_{water} is the volume of water in the soil matrix and V_{voids} is the volume of voids.

106 Unless otherwise stated, the sample preparation consisted of the following three steps:

107 1) Alternating injection of equal volumes of bacterial suspension and cementation
108 solution with an inflow rate of about 1 L/hour. The total volume of the introduced
109 solutions was the same as the aforementioned water volume so as to keep a
110 constant degree of saturation. A vacuum pump was connected to the bottom of the
111 PVC column to remove the excess solution.

112 2) Curing for 12 hours at $25\pm 1^\circ\text{C}$ to allow the bacterial fixation process to complete.

113 3) Percolation of cementation solution with the same flow rate followed by another
114 curing period of 12 hours at $25\pm 1^\circ\text{C}$. This step was carried out twice.

115 It should be noted that, to obtain different mechanical properties of the soil samples, the
116 above-mentioned three steps might be conducted more than once.

117 The key issue of the above process is to keep a constant degree of saturation throughout
118 the tests by managing the volume of extracted solution to be equal to that of the injected
119 solution. Meanwhile, to avoid solution accumulation at the bottom of the sand column
120 by gravity, the PVC columns were horizontally placed during the curing period. The
121 saturation degrees over the entire 15 cm long sand columns were determined. The local
122 saturation of the columns between 2.5 to 12.5 cm depth was relatively homogeneously
123 distributed with a deviation not greater than $\pm 6\%$ saturation. Therefore, the specimens
124 prepared for the mechanical property analyses were taken from about 2 to 13 cm depth
125 of the sand columns.

126 **2.4 Microscopy Investigation**

127 In order to characterize the shapes and locations of the precipitated CaCO_3 and to
128 investigate the bonding behaviour between the grain hosts and cement agent,
129 microscopy analysis was conducted on the cemented soil samples, which were taken
130 from the centre of the cemented sand columns. Before conducting the microscopy
131 investigation, all samples were flushed with tap water and dried at 60 °C for 24 hours.
132 The microscopy investigation was carried out using scanning electron microscopy
133 (SEM) PHILIPS XL20 Scanning Electron Microscope, Eindhoven, the Netherlands.

134 **2.5 Unconfined Compressive Strength (UCS) Tests**

135 To quantify the strength imparted into the MICP treated silica sand under different
136 saturation conditions, the unconfined compressive strength (UCS) tests were conducted
137 on cemented specimens of 55 mm in diameter with a selected diameter to height ratio of
138 1:1.5 to 1:2. The axial load was applied at a constant rate of 1.0 mm/min. Before
139 carrying out the tests, the sand samples were treated with different amounts of MICP
140 under 20%, 40%, 80% and 100% degrees of saturation.

141 **2.6 Triaxial Compression Tests**

142 The triaxial compression test was employed to provide verification for the MICP as a
143 soil stabilization technique. This test is considered to be the most reliable test to
144 measure the shear strength parameters of soils. In this study, a series of single-stage
145 consolidated undrained triaxial tests with pore water pressure measurement were carried
146 out to establish the effective shear strength parameters (i.e., cohesion, c' , and friction
147 angle, ϕ') of the bio-cemented sand. Specimens were set under one confining pressure

148 and sheared till failure. The effective cohesion and friction angle were determined using
149 the Mohr-Coulomb failure envelopes established from three individual samples. All
150 tests were conducted in accordance with the procedures set out by Head (1998). Before
151 carrying out the triaxial tests, the bio-cemented specimens were treated at different
152 degrees of saturation of 30%, 65% and 100%. Each triaxial test started with saturating
153 the sand specimens with tap water so as to achieve a Skempton's B value of at least
154 95%. The specimens were then subjected to confining pressures of 50, 100 and 200 kPa,
155 respectively, and an axial stress was then applied to failure at a strain rate of 1 mm/min.
156 All triaxial tests were performed on specimens of 55 mm in diameter with a selected
157 diameter to height ratio of approximately 1:2. A baseline sample of untreated sand was
158 also tested to allow comparison of the soil improvement properties.

159 **2.7 Permeability Tests**

160 Permeability is a primary factor that controls the behavior of porous materials under
161 saturated conditions and thus dictates the suitability of a specific material for certain
162 applications (Shahin et al. 2011). Porous materials with high permeability can prevent
163 the development of excess pore water pressure during loading. To identify the
164 permeability of cemented sand treated with different amounts of CaCO_3 precipitates,
165 more samples were prepared at degrees of saturation of 30%, 65% and 100%, and
166 permeability tests were conducted. The permeability test was also conducted on the
167 untreated samples for the purpose of comparison with the treated samples. The
168 untreated fine sand has a hydraulic conductivity of 9.2×10^{-5} m/s, whereas it is $44.7 \times$
169 10^{-5} m/s for the untreated coarse sand.

170 Laboratory determination of the permeability of the untreated and bio-cemented sand
171 was conducted using constant head permeability test with a rigid side wall device in
172 accordance with the Australian Standards AS 1289 (2007). All specimens were
173 saturated prior to the permeability test by flushing through 2 L tap water under 15 kPa
174 back pressure (hydraulic head of about 150 cm) to remove most of the remained pore
175 air.

176 In order to compare the permeability of the MICP improved soil with conventional soil
177 improvement using chemical additives, a series of mixtures of fine sand with various
178 proportions of Portland cement were prepared and tested for their strength and
179 permeability. The details of the Portland cement samples are listed in Table 1. The
180 mixtures were poured into PVC columns with the same dimension of that used for bio-
181 cementation, and a strong vibration was applied to avoid any air bubbles that might
182 remain in the mixture. The prepared mixtures were then cured at the room temperature
183 (20 ± 1 °C) for 7 days prior to the UCS and permeability measurements.

184 **2.8 Durability Tests**

185 **2.8.1 Freeze-Thaw Durability**

186 To test the resistance of MICP cemented samples to freeze-thaw (FT) cycling, a series
187 of fine sand samples (110 mm in height and 55 mm in diameter) treated by MICP and
188 Portland cement, as described previously, was subjected to 10 cycles of FT actions.
189 Each cycle test involves subjecting the samples to a 12-hour freeze at -14 °C followed
190 by a 12-hour thaw under ambient conditions (20 ± 1 °C). All samples were immersed in
191 water throughout the cycling FT testing.

192 2.8.2 Acid Rain Durability

193 Artificial acid rain was made according to Haneef et al. (1992) and the final pH of acid
194 rain was adjusted to 3.5 by adding additional H₂SO₄. The artificial acid rain was
195 injected from the top of the cemented fine sand columns (180 mm in height and 55 mm
196 in diameter) with a flow rate of approximately 3 mL/min. The weight of the sand
197 column was measured periodically, after it was washed by DI water and dried at 105 °C
198 for 12 hours. All samples were cut in half prior to the shear strength test and the
199 strength of the top and bottom parts of the sand samples (eroded and un-eroded) was
200 recorded.

201 3 Presentation of Results

202 3.1 Effect of Degree of Saturation on UCS Results of MICP Cemented Coarse 203 Sand

204 Figures 2 and 3 show the results of the UCS tests carried out on the coarse sand treated
205 with different amounts of MICP under various saturation degrees of 20%, 40%, 80%
206 and 100%. It can be seen that both unconfined compressive strength (q_{ucs}) and stiffness
207 (or elastic modulus, E) increase with the increase of CaCO₃ content for all treated
208 samples. Both q_{ucs} and E follow exponential relationships with the content of CaCO₃,
209 which are in line with previous results reported by van Paassen et al. (2010). It can also
210 be seen that for the same amount of CaCO₃ precipitation, both q_{ucs} and E increase with
211 the reduction in the degree of saturation. Saturation degree higher than 80% was found
212 to have little impact on q_{ucs} and E of MICP treated coarse sands.

213 It is worthwhile mentioning that the failure mechanism of the cemented sand was
214 different from the strong to the weak samples. In the weak samples, the broken cores
215 completely lost strength at the grain scale around the failure plane, or through the entire
216 sample when the failure planes were not clear. This was consistent with previous
217 observation by van Paassen et al. (2009). In the strong samples, however, tensile cracks
218 appeared vertically from top to bottom along the sample and the failure planes can be
219 distinguished clearly, which was also similar to the previous observation by van
220 Paassen et al. (2009).

221 It is of interest to examine the location of MICP treated coarse silica sand in the
222 spectrum of other geomaterials in terms of the relationship between E and q_{ucs} , as shown
223 in Figure 4. The change in the rigidity of the MICP treated silica sand is also shown in
224 Figure 5 (rigidity = $E/q_{ucs} = 1/\varepsilon_f$, where ε_f is the axial strain at failure). It can be seen that
225 the rigidity increases (in an exponential law fashion) with increase of CaCO_3 content,
226 but was independent of the degree of saturation. It can also be seen that at similar
227 amount of CaCO_3 , the rigidity of the samples cemented at lower degree of saturation
228 was higher than that of the samples treated with higher degree of saturation. Similar to
229 the effect of saturation on q_{ucs} , a degree of saturation higher than 80% had marginal
230 impact on the rigidity of MICP cemented sand for certain amount of CaCO_3 content.

231 **3.2 Microscopy Images of MICP Cemented Sand at 20% and 100% Saturation**

232 In this part, an attempt is made to investigate the reason for increasing strength and
233 stiffness of the MICP treated sand at lower degree of saturation. It is believed that the
234 micro-features of precipitated crystals around the sand grains and the creation of hinges
235 can be responsible for the different mechanical responses of MICP treated porous

236 materials obtained at different saturation conditions (Paraskeva et al. 2000). In order to
237 investigate this matter, the micro-structure of the treated sands was investigated through
238 the microscopy images shown in Figures 6 and 7 for soil treated at degrees of saturation
239 of 100% and 20%, respectively.

240 It can be seen from the images shown in Figure 6 that the CaCO_3 crystals produced at
241 100% saturation take rhombohedron form in which the agglomerated rhombohedral
242 crystals precipitate not only in the inter-particle contact points but also on the grain
243 surface, or suspend in the pore spaces, leading to insufficient connections between the
244 sand grains. For the sand treated at 20% saturation (Figure 7), a strong coating effect of
245 the MICP process is predominant. This coating effect is likely attributed to the
246 homogeneously adsorbed solution on the sand grains surface due to the surface tension
247 force, which allows the MICP solution to access the full surface of the grains. One
248 important feature that can be derived from Figure 7 is that the gaps between the host
249 grains are almost completely filled with crystals, which is likely due to the fact that the
250 retained MICP solution located between the grains takes a menisci form, where the
251 crystals are produced and precipitated out of the aqueous solution to fill the gaps. This
252 feature may affect the adhesion mechanism amongst the host grains and, consequently,
253 the mechanical behavior of the entire soil matrix.

254 It should be noted that both samples treated at 100% saturation (Figure 6) and 20%
255 saturation (Figure 7) demonstrate similar q_{ucs} of 1 MPa and 1.14 MPa, respectively,
256 but they differ in the CaCO_3 content. It is apparent that the development of the CaCO_3
257 at the contact boundary is vastly different in both cases, and in comparison it can be
258 identified that an excess precipitation of the CaCO_3 at the sand grain boundary exists for

259 the case of 100% saturation condition. As a result, the sample treated at 20% saturation
260 contained fewer CaCO_3 crystals less than half of that precipitated at 100% saturation
261 (i.e. 0.143 g/g sand). This indicates that the mechanical strength of the MICP treated
262 samples is due to the effectiveness of CaCO_3 formation that precipitated in the inter-
263 particles contact points, rather than the total amount of the CaCO_3 crystals formed.

264 The schematic diagram shown in Figure 8 can provide further explanation of the
265 previous observation. For partially saturated condition, the air occupies the center of the
266 pores and the total surface of the grains is covered with adsorbed solution, which is
267 predominantly concentrated at the inter-particles connection points (corner) forming
268 menisci shape (Tuller et al. 1999). Therefore, the crystal precipitation has mainly
269 occurred at the contact points of the grains (Figure 8), which contributes to the strength
270 improvement. In the case of full saturation, as the MICP solution occupies the entire
271 pore space, the crystals are free to precipitate without being restricted to the size and
272 location, resulting in the agglomerated crystals to be formed on both the host grain
273 surface and grain gaps. From the above discussion, it can be stated that the crystals
274 formation varies in size and location according to the distribution of pore solution,
275 which is influenced by the saturation conditions.

276 **3.3 Mathematical Model of Total Volume of Effective Hinges**

277 In Sections 3.2 and 3.3, it was experimentally shown (through microscopy images and
278 results of UCS tests) that the degree of saturation at which a sand soil is treated by
279 MICP has a significant impact on the resulting strength and stiffness. Also the particle
280 size of the constituent soil affects the cementation process, because it has a significant
281 impact on the retained pore water in terms of the content, shapes and distribution under

282 various saturation conditions, consecutively on the cementation process. In this section,
283 a mathematical model is developed in order to measure the impact of the saturation
284 degree and particle size on the effective “hinge” formation within a soil matrix treated
285 with MICP.

286 In order to develop the mathematical model, a soil matrix with uniform spherical
287 particles is assumed. All spherical particles are packed in a tetrahedral packing form
288 having the closest packing order with a void ratio of 0.34. The total volume of the sand
289 matrix (V) and void volume (V_{void}) can be approximately calculated as follows:

290 [4]
$$V = N \times (4/3) \times \pi \times R^3 / (1 - 0.34)$$

291 [5]
$$V_{void} = 0.34 \times V$$

292 where; N is the number of particle spheres and R is the radius of the sphere (see Figure
293 9).

294 In the assumed tetrahedral packing, each particle has 12 contact points with the
295 surrounding particles and there are 6 full water lenses in each unit volume of $5.66R^3$ (Lu
296 and Likos 2004). The total number of water lenses (N_{lens}) in the sand matrix therefore
297 can be calculated as follows:

298 [6]
$$N_{lens} = 6 \times V / (5.66 \times R^3)$$

299 The crystals are assumed to be homogeneously precipitated on the surface of spheres,
300 where the water lenses are attached, and the crystal “hinges” formed in point-to-point

301 contacts contribute to the bonding force. In general, it is reasonable to make the
 302 hypothesis that the bigger volume of “hinges” causes stronger bonding force. From
 303 Figure 9b, the total volume of effective hinges ($V_{T-hinges}$) in the soil matrix can be
 304 calculated as follows:

$$305 \quad [7] \quad V_{T-hinges} = N_{lens} \times V_{hinge} = N_{lens} \times (2\pi \times r^2 h' - 2\pi / 3 \times h'^2 (3r - h'))$$

306 where; V_{hinge} presents the volume of each hinge, and h' & r are as illustrated in Figure
 307 9b, which can be obtained based on the following geometric calculations:

$$308 \quad [8] \quad h' = R - \sqrt{R^2 - r^2}$$

$$309 \quad [9] \quad r = \sqrt{(R + h)^2 - R^2}$$

310 In Eqns. 8 and 9, h is the thickness of crystals on each sphere and can be estimated as
 311 follows:

$$312 \quad [10] \quad h = V_{crystals} / (2 \times S_{surface})$$

313 where; $V_{crystals}$ is the volume of CaCO_3 crystals precipitated on each sphere and $S_{surface}$ is
 314 the contact surface between the water lens and the sphere (see Figure 9a and b). Both
 315 $V_{crystals}$ and $S_{surface}$ can be calculated according to the following expressions:

$$316 \quad [11] \quad V_{crystals} = C_{crystals} \quad V / \quad crystal \quad / N_{lens}$$

$$317 \quad [12] \quad S_{surface} = 2\pi \times (R + h)^2 \times (R - (R + h) \times \cos(\theta))$$

318 where; $C_{crystals}$ is the CaCO_3 crystals content (g/cm^3) and $\rho_{crystals}$ is density of CaCO_3
319 crystals (i.e. 2.71 g/cm^3).

320 The degree of saturation of the soil matrix can also be obtained as follows:

321 [13]
$$S_{saturation} \% = V_{water} / V_{void} = N_{lens} \times V_{lens} / V_{void}$$

322 where; V_{lens} is the volume of each water lens, which can be calculated in accordance
323 with Dallavalle (1943), as follows:

324 [14]
$$V_{lens} = 2\pi \times R^3 \times (1/\cos(\theta) - 1)^2 \times [1 - (\pi/2 - \theta) \times \tan(\theta)]$$

325 The developed mathematical model (i.e. Eqns. 7 and 14) was used to illustrate the
326 dependency of the total volume of effective “hinges” formed in the same volume of
327 sand matrixes on the degree of saturation and particle size (see Figure 10). The number
328 of spherical particles, N , is inversely proportional to the particle size (R), providing the
329 same total matrix volume. This means that if the coarse sand particle has a radius R
330 while the fine sand particle has a radius $R/2$, the number of particles of the fine sand
331 will be eight times that of the coarse sand. Consequently, the total number of water
332 lenses (N_{lens}) in the fine sand matrix will be eight times that of the coarse sand.

333 The model predictions shown in Figure 10 indicate that a greater volume of effective
334 hinges is formed in the fine sand compared to the coarse sand having similar amount of
335 CaCO_3 precipitation, indicating that the strength is improved with the decrease in
336 particle size. This model also derives that a lower degree of saturation leads to a greater
337 number of effective hinges at the same CaCO_3 content and consequently an improved

338 mechanical behavior (i.e. UCS). The model predictions are supported by the previous
339 experimental UCS tests and microscopy images of the coarse sand.

340 To further investigate the real effect of particle size and degree of saturation on the
341 shear strength parameters of treated sand (i.e., cohesion, c' , and friction angle, ϕ'),
342 which are more relevant to most geotechnical engineering applications, the results of the
343 undrained triaxial tests are presented below.

344 **3.4 Mechanical Behavior of Stabilized Sand in Triaxial Tests**

345 The effective shear strength parameters (i.e. cohesion, c' , and friction angle, ϕ') of the
346 silica sand treated with different amounts of CaCO_3 were determined from the Mohr-
347 Coulomb envelopes. These were developed from the peak shear stress values obtained
348 from the triaxial tests. Results are shown in Figures 11 and 12, for coarse and fine
349 sands, respectively.

350 **Coarse Sand**

351 Figure 11 shows that both the cohesion, c' , and friction angle, ϕ' , increase with the
352 increase of the CaCO_3 content at all degrees of saturation. At a fixed amount of CaCO_3
353 a lower saturation degree increased the c' and ϕ' values compared to those at higher
354 saturation degrees. Under lower saturation degree condition, the precipitated crystals
355 contributed more to improving cohesion than to improving friction angle. At higher
356 saturation degrees of 65% and 100%, the impact on improving the friction angle was
357 even less. As mentioned earlier, the effect of degree of saturation on improving the
358 shear strength behavior of soil and thus the shear strength parameters is attributed to

359 restricting the crystal formation mainly to the connection points. The well-placed
360 crystals are efficient in increasing the inter-particle connection, thereby, enhancing the
361 soil cohesion and friction angle. The increase in both cohesion and friction angle at
362 higher CaCO₃ content that has occurred regardless of the saturation degree is likely due
363 to the fact that precipitated crystals start filling the pore spaces. One important feature
364 that can be derived from Figure 11 is that at low CaCO₃ content the friction angle had
365 only marginally increased under all saturation conditions, which was probably due to
366 the slight increase in the dry density. The optimum condition for c' and ϕ' has occurred
367 at the saturation condition of 30%.

368 **Fine Sand**

369 Figure 12 shows that the overall correlation between the shear strength parameters and
370 the CaCO₃ content at different saturation degrees is similar to that of the coarse sand.
371 By comparing the results of the two sands used, it can be concluded that under the same
372 saturation condition, the coarse sand demonstrates higher friction angle than the fine
373 sand at similar CaCO₃ content. The fine sand with similar CaCO₃ content showed
374 significantly higher values of cohesion compared to the coarse sand. This can be
375 explained as follows. Smaller particles have two effects including: (a) providing more
376 inter-particle contact points for microbially induced CaCO₃ to precipitate; and (b)
377 reducing the stress acting per particle contact. MICP acts most efficiently at a particle
378 contact just as cementation begins, and continued expansion of cementation around a
379 particle contact has decreased effect. Therefore, reallocating the CaCO₃ crystals to two
380 contact locations instead of one would be more effective. At the same time, the contact
381 stress decreases as a function of the particle radius squared. Therefore, smaller particles

382 provide two compounding benefits: (1) more efficient MICP; and (2) lower particle
383 contact stresses.

384 **3.5 Effect of MICP Treated Sand on Permeability**

385 Figure 13 shows the results of permeability tests conducted in the current study. It can
386 be seen that a reduction in permeability was encountered for all bio-cemented sand
387 samples. In contrast to the phenomenon reported by Whiffin et al. (2007), the
388 permeability decreased with an increase in CaCO_3 content for both fine and coarse
389 sands, irrespective of the saturation degree. Results suggest that it is preferable to
390 conduct the MICP process under lower saturation conditions, as it enabled improved
391 mechanical behavior at the same time as maintaining relatively high residual
392 permeability.

393 Figure 14 shows the results of comparison between sand samples treated with Portland
394 cement and bio-cement. It can be seen that the bio-cement samples have higher strength
395 in the range of lower cement agents content (< 0.1 g/g sand) compared to the Portland
396 cement samples after 7 days of curing. However, this comparison would differ
397 depending on the applied curing time of the Portland cement samples. The permeability
398 of the biocementation samples is significantly higher than that of the Portland cement
399 samples. As an example, a mixture with 7% (0.07 g/g sand) Portland cement
400 dramatically decreased permeability by 98%. Cement content higher than 9.6% (0.096
401 g/g sand) produced a poor drainage material with permeability less than 1×10^{-6} m/s.
402 The significant loss of permeability in the Portland cement samples is due to the
403 occupation of the pore space by the water insoluble hydrates formed from the cement
404 hydration reaction with the pore water. In contrast, the loss of permeability in bio-

405 cement samples is caused by the pore spaces becoming occupied by the calcite crystals,
406 which only causes a smaller volume change compared to the hydrates.

407 From the previous results, it can be concluded that apart from the significant increase in
408 soil strength and stiffness, one advantage of biocementation is attributed to the relative
409 ability to retain soil permeability after treatment, compared to the traditional chemical
410 treatment by Portland cement.

411 **3.6 Effect of MICP Treatment on Sand Freeze-Thaw Durability**

412 Destruction of porous materials caused by freezing and thawing has been of great
413 concern to engineers for more than 200 years (Johnson 1952). The phase change of
414 water adsorbed in the soil pores is the most significant cause of deterioration of exposed
415 porous materials. Porous solids with high porosity or permeability usually have a good
416 service record after free-thaw (FT) action (Litvan 1980). Indicated by the previous
417 permeability results, the sand samples treated with MICP have a high residual
418 permeability, which may favor the samples to endure the cycled FT action.

419 By comparing the UCS of MICP tested samples before and after FT cycling, less than
420 10% decrease in strength occurred irrespective of the treatment conditions (Figure 15).
421 The severity of the mechanical damage is proportional to the water content of the
422 porous solid (Litvan 1980); however, the high porosity and permeability allow more
423 rapid water mass transfer in the sand matrix, which can increase the FT resistance. For
424 MICP samples, the crystals formed at the contact points can maintain the connection of
425 pores without restricting the pore water mobility, which is also proved by the previous

426 permeability tests. For the Portland cement samples, the FT cycles caused serious
427 damage, as expected, with about 40% decrease in strength.

428 **3.6.1 Acid Rain Erosion Durability**

429 Acid rain is detrimental to many construction materials, particularly those made from
430 limestone or sand stone with high CaCO₃ content. The chemical reaction between the
431 calcium carbonate and sulfuric acid (the primary acid component of acid rain) causes
432 the dissolution of CaCO₃, resulting in destruction of such materials. In the MICP treated
433 sand, the strength of sand matrix is the result of the sand particles bonded by the
434 bridging CaCO₃ crystals. Therefore, the CaCO₃ crystals eroded by the acid rain will
435 result in destruction of the connections between the sand particles, leading to severe
436 damaging in mechanical properties.

437 In order to test erosion and residual strength of the MICP treated sand samples after
438 exposure to the acid rain, in time mass detection of the sand matrix and UCS tests were
439 carried out and the results are presented in Figure 16. It can be seen that, as expected,
440 the artificial acid rain (pH=3.5) continuously eroded the biocement samples, resulting in
441 a loss of weight. The pH of the effluent stayed around 7.5, which indicated that the
442 protons (H⁺) in the acid rain were consumed by reacting with CaCO₃, similar to the acid
443 rain erosion of limestone and marble. After flushing 12 L of acid rain through the sand
444 column, corresponding to 5 years of rainfall (1000 mm/year), the UCS results of the
445 eroded samples reflected that no obvious damage occurred at the bottom part of the
446 sand column (9-18 cm). However, the strength of the top part of the sand column was
447 decreased by about 40%, as shown in Figure 16. As the effect of the acid rain is chronic

448 and long-term acidification results from years of acidic rainfall, a long-term simulation
449 experiment (decades) is worthwhile to carry out in the future.

450 **4 Discussion**

451 This study verified that the bio-cementation technology applied to partially saturated
452 soils lead to improved mechanical behavior of MICP treated soil matrix in terms of
453 cohesion, friction angle and UCS, with fewer calcite crystals compared to MICP at fully
454 saturated condition. In other words, to produce similar soil strength, partially saturated
455 soils require fewer crystals, enabling bio-cemented soils to be produced more
456 economically due to lower requirement for the urease enzyme, urea and CaCl_2 . To this
457 end, the technique can be applied to many geotechnical-engineering applications in both
458 fully and partially saturated conditions. In wet fully saturated condition, MICP solution
459 is introduced into the soil by saturated flow (van Paassen et al. 2010; Whiffin et al.
460 2007). In dry or partially saturated condition, MICP solution can be introduced by
461 surface percolation and the excess of MICP solution moves deeper into the soil pores,
462 which allows the retained MICP solution to accumulate at the connection points as a
463 meniscus shape (Cheng and Cord-Ruwisch 2012). The restricted distribution of MICP
464 solution enables the crystals formed at the particular position, which contributes the
465 most to strength development. However, an obvious main challenge for MICP treatment
466 under unsaturated conditions is achieving homogenous distribution of CaCO_3 and
467 strength, which will be investigated in subsequent phase of this work.

468 A principal engineering problem produced by current available soil improvement
469 methods is the tendency of significantly decreasing permeability of treated soils. For

470 example, the reduction in permeability due to grouting ranges between 2 and 3 orders of
471 magnitude (Karol 2003). Consequently, the reduction in permeability disturbs natural
472 groundwater flow paths, permits the increase of pore water pressure in the soil, thus
473 increasing the risk of failure in both earth and foundation structures. The ability of
474 MICP to retain high permeability conditions is a clear advantage compared to the
475 alternative of using Portland cement. A reduction in the cost of construction and
476 installation of drainage systems would be apparent, as fewer systems would need to be
477 integrated than those typically utilizing traditional cementing agents. Another advantage
478 of MICP and its retention of *in-situ* permeability during bio-cementation application is
479 that it will permit additional applications of treatment allowing engineers to control the
480 final strength.

481 Engineering examples of the utilization of MICP and the associated benefits of
482 permeability retention would be in the reinforcement of transport subgrades and
483 embankments. During subgrade construction it is important to provide adequate
484 drainage at all times to prevent water from standing on the subgrade. Therefore, soil
485 stabilization by MICP technique with the capability of high permeability retention
486 would eliminate the need for additional drainage systems. Due to the minimal
487 interference with soil material hydrology, embankments strengthened with MICP will
488 have the potential to allow immediate dissipation of excess pore water pressures caused
489 by operational surcharge loads.

490 Geotechnical engineering structures exposed to dynamic loads associated with
491 earthquakes under saturated conditions can be subject to significant structural damage.
492 In this case, the soil loses most of its static strength and significant deformations occur.

493 When such deformations are large, soils liquefy (Cornforth 2005). The soil types most
494 susceptible to liquefaction are loose granular sands that have no cementation between
495 the soil grains. Given the improvements in the undrained shear strength of sands trialed
496 in this study, MICP can be used as a viable solution to improve the properties of un-
497 cemented granular soils by creating cemented zones that will be no longer liquefiable.

498 **5 Conclusions**

499 This paper has investigated the influence of degree of saturation and soil particle size on
500 the mechanical response of calcite bio-cemented silica sand. Samples examined under
501 SEM indicated different patterns of calcite precipitation for each degree of saturation,
502 with fully saturated condition forming agglomerated rhombohedral crystals scattered on
503 the sand grain surface. The lower saturated conditions formed strong calcite coating on
504 the host grains and bridging between sand grains. A mathematical model has been also
505 developed, which measures the impact of the degree of saturation and particle size on
506 the effectiveness of CaCO_3 precipitates in MICP treated soils.

507 Findings of this study confirmed that higher strengths were obtained at lower saturation
508 degrees, challenging most studies on MICP so far, in which biocementation was
509 performed under fully saturated condition. This important finding indicates that
510 optimum performance of this stabilization process can be achieved with lower costs,
511 making it economically viable while reducing the need for water and chemicals, hence,
512 becoming more environmentally sustainable than formerly believed.

513 The results from the durability tests have shown that MICP produced cemented samples
514 with highly durable resistance to freeze-thaw erosion, and resistless to the acid rain

515 erosion. Both the permeability and shear strength of bio-cemented soils displayed
516 results that would support the MICP as a promising soil improvement technique. MICP
517 has been approved to be a viable alternative for engineering soil improvement
518 applications such as soil embankments, liquefiable sand deposits and subgrade
519 reinforcement.

520 The results obtained from the UCS and triaxial tests have shown that, despite having the
521 same amount of calcite crystals, the engineering response of treated sand varies
522 significantly, mainly because of the different location of the calcite deposited. The
523 calcite crystals formed under lower degree of saturation showed that more crystals are
524 formed in the contact points, which contributed to the strength of the cemented samples.

525 **6 Acknowledgement**

526 The authors would like to acknowledge Deltares (the Netherlands) and University of
527 Murdoch (Australia) for the financial support given to this project. The authors would
528 also like to thank Atticus Dekuyser for providing assistance in the triaxial measurements.

529 **7 References**

530 Australian Standards AS 1289, 2007. Method of testing soils for engineering purposes.

531 Al-Thawadi, S., and Cord-Ruwisch, R. 2012. Calcium carbonate crystals formation by
532 ureolytic bacteria isolated from Australian soil and sludge. *Journal of Advance Science
533 and Engineering Research*, 2 (1): 13-26.

534 Barla, M., Barla, G., Lo Presti, D.C.F., Pallara, O., and Vandebussche, N. 1999.
535 Stiffness of soft rocks from laboratory tests. *Proceedings of the IS Torino '99*, 2nd
536 International Symposium on Pre-failure deformation characteristics of

- 537 geomaterials. Torino, 26-29 September 1999.
- 538 Burbank, M.B., Weaver, T.J., Green, T.L., Williams, B.C., and Crawford, R.L. 2011.
539 Precipitation of calcite by indigenous microorganisms to strengthen liquefiable soils.
540 Geomicrobiology Journal, 28(4): 301-312.
- 541 Cheng, L., and Cord-Ruwisch, R. 2012. *In-situ* soil cementation with ureolytic bacteria
542 by surface percolation. Ecological Engineering, 42: 64-72.
- 543 Cornforth, D.H. 2005. Landslides in practice: investigation, analysis, and
544 remedial/preventative options in soils. John Wiley & Sons, Inc.
- 545 Dallavalle, J.M. 1943. Micrometrics. Pitman, London.
- 546 DeJong, J. T., Fritzsche, M. B., and Nusslein, K., 2006. Microbially Induced
547 Cementation to Control Sand Response to Undrained Shear. Journal of Geotechnical
548 and Geoenvironmental Engineering, 132 (11): 1381- 1392.
- 549 DeJong, J. T., Mortensen, B. M., Martinez, B. C., and Nelson, D. C. 2010. Biomediated
550 soil improvement. Ecological Engineering, 36 (2): 197-210.
- 551 Haneef, S.J., Dickinson, C., Johnson, J.B., Thompson, G. E., and Wood, G.C. 1992.
552 Simulation of the degradation of coupled stones by artificial rain. Studies in
553 Conservation, 37(2): 105-112.
- 554 Head, K.J.H. 1998. Manual of Soil Laboratory Testing. John Wiley and Sons,
555 Chichester, England.
- 556 Ismail, M.A., Joer, H.A., Randolph, M.F., and Meritt, A. 2002a. Cementation of porous
557 materials using calcite. Géotechnique, 52(5): 313-324.
- 558 Ismail, M.A., Joer, H.A., Sim, W. H., and Randolph, M.F. 2002b. Effect of cement type
559 on shear behavior of cemented calcareous soil. Journal of Geotechnical and
560 Geoenvironmental Engineering, 128(6): 520-529.
- 561 Johnson, A.W. 1952. Frost action in roads and airfield-a review of the literature. Special
562 Report No. 1, Highway research board, Washington, D.C.

- 563 Karol, R. H. 2003. Chemical Grouting and Soil Stabilization. New York, Marcel
564 Dekker.
- 565 Litvan, G.G. 1980. Freeze-thaw durability of porous building materials, durability of
566 building materials and components. ASTM STP 691. P. J. Sereda and G. G. Litvan,
567 Eds, American Society for testing and materials, 1980, pp. 455-463.
- 568 Lu, N., and Likos, W.J. 2004. Unsaturated soil mechanics. John Wiley & Sons, Inc.
569 New Jersey.
- 570 Mitchell, A., and Ferris, F. 2006. The influence of bacillus pasteurii on the nucleation
571 and growth of calcium carbonate. Geomicrobiology Journal, 23(3-4): 213-226.
- 572 Paraskeva, C.A., Charalambous, P.C., Stokka, L.E., Klepetsanis, P.G., Koutsoukos,
573 P.G., Read, P., Ostvold, T., and Payatakes, A.C. 2000. Sandbed consolidation with
574 mineral precipitation. Journal of Colloid and Interface Science, 232: 326-339.
575 doi:10.1006/jcis.2000.7161
- 576 Shahin, M.A., Mardesic, T., and Nikraz, H.R. 2011. Geotechnical characteristics of
577 bauxite residue sand mixed with crumbed rubber from recycled car tires. Journal of
578 GeoEngineering, 6(1): 63-72.
- 579 Tuller, M., Or, D., and Dudley, L.M. 1999. Adsorption and capillary condensation in
580 porous media: liquid retention and interfacial configurations in angular pores. Water
581 Resource Research, 35 (7): 1949–1964.
- 582 van Paassen, L.A., Ghose, R., Van der Linden, T.J.M., Van der Star, W.R.L., and Van
583 Loosdrecht, M.C.M. 2010. Quantifying biomediated ground improvement by ureolysis:
584 large-scale biogrout experiment. Journal of Geotechnical and Geoenvironmental Engineering,
585 136(12): 1721-1728.
- 586 van Paassen, L.A., van Loosdrecht M.C.M., Pieron, M., Mulder, A., Ngan-Tillardm
587 D.J.M., and van der Linden, T.J.M. 2009. Strength and deformation of biologically
588 cemented sandstone. proceedings of the ISRM Regional conference EUROCK 2009-
589 Rock engineering in difficult ground conditions- Soft rocks and karst, 29-31 October
590 2009, Dubrovnik, Croatia, pp. 405-410.

- 591 Warren, A.A., Maurice, P.A., Parmar, N., and Ferris, F.G. 2001. Microbially mediated
592 calcium carbonate precipitation: Implications for interpreting calcite precipitation and
593 for solid-phase capture of inorganic contaminants. *Geomicrobiology journal*, 18(1): 93-
594 115.
- 595 Whiffin, V.S., van Paassen, L.A., and Harkes, M.P. 2007. Microbial carbonate
596 precipitation as a soil improvement technique. *Geomicrobiology Journal*, 24(5): 417-
597 423.

598

Table 1. Mix proportions of Portland cement samples.

| Mix ID | Cement (g) | Sand (g) | Water (mL) | Density (g/cm³) |
|---------------|-------------------|-----------------|-------------------|-----------------------------------|
| 1 | 40 | | | |
| 2 | 56 | | | |
| 3 | 72 | 580 | 124 | 1.93±0.01 |
| 4 | 84 | | | |

599

600 **Figure Captions:**

601

602 **Figure 1.** Grain size distribution curves for the sand used.

603 **Figure 2.** Variation of UCS with CaCO_3 content and different saturation conditions for
604 coarse sand.

605 **Figure 3.** Variation of stiffness with CaCO_3 content and different saturation conditions
606 for coarse sand.

607 **Figure 4.** Relationship between elastic modulus (E) and q_{ucs} of the MICP treated silica
608 sand compared with other geomaterials.

609 **Figure 5.** Relationship between rigidity and CaCO_3 content for silica sand treated with
610 MICP under different water saturation degree conditions.

611 **Figure 6.** Formation of CaCO_3 crystals for samples treated at 100% saturation (note:
612 CaCO_3 content = 0.143 g/g sand, UCS = 1 MPa).

613 **Figure 7.** Formation of CaCO_3 crystals for samples treated at 20% saturation (note:
614 CaCO_3 content = 0.057 g/g sand, UCS = 1.14 MPa).

615 **Figure 8.** Conceptual illustration of pore cementation solution distributed in the sand
616 matrix under different saturation conditions.

617 **Figure 9.** Schematic diagram of two-dimensional meniscus between spherical particles:
618 (a) water lens between two particles; and (b) simple two-dimensional geometrical
619 illustration of hinge formation between two particles.

620 **Figure 10.** Results of mathematical model showing the correlation of the CaCO_3
621 content and volume of effective hinges within the soil matrix for coarse and fine sands
622 (R_{CS} and R_{FS} represent the radii of the coarse and fine particles, N represents the
623 number of particle spheres.).

624 **Figure 11.** Effect of saturation conditions on shear strength parameters of coarse silica
625 sand having different amount of CaCO_3 .

626 **Figure 12.** Effect of saturation conditions on shear strength parameters of fine silica
627 sand having different amount of CaCO_3 .

628 **Figure 13.** Permeability of cemented sand columns treated at different saturation
629 conditions for: (a) coarse sand; and (b) fine sand.

630 **Figure 14.** UCS and permeability of sand samples cemented with bio-cement CaCO_3
631 (100% saturation) and Portland cement.

632 **Figure 15.** UCS of cemented fine sand samples before and after 10 cycles of Freeze-
633 Thaw (FT) action (one cycle per day). (Note: CaCO_3 content was about 0.06-0.065 g/g
634 sand and Portland cement content was 0.096 g/g sand).

635 **Figure 16.** UCS and loss of weight of MICP cemented fine sand samples during the
636 acid rain erosion experiments (Note: sand columns were treated under fully saturated
637 condition with CaCO₃ content of about 0.1-0.105 g/g sand).

Fig. 1

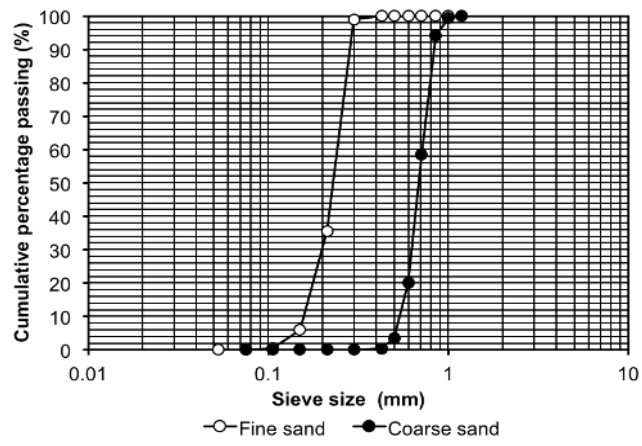


Fig. 2

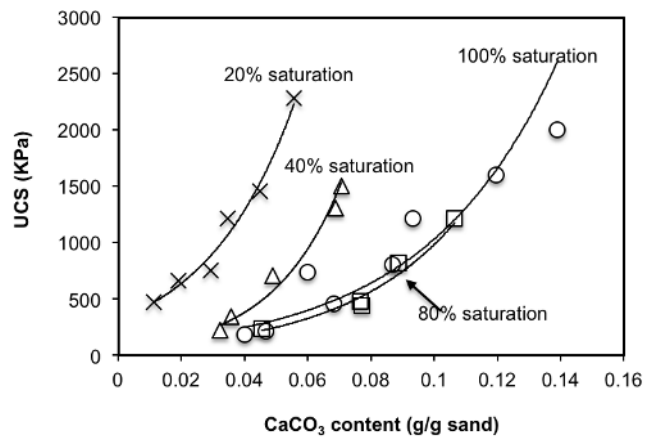


Fig. 3

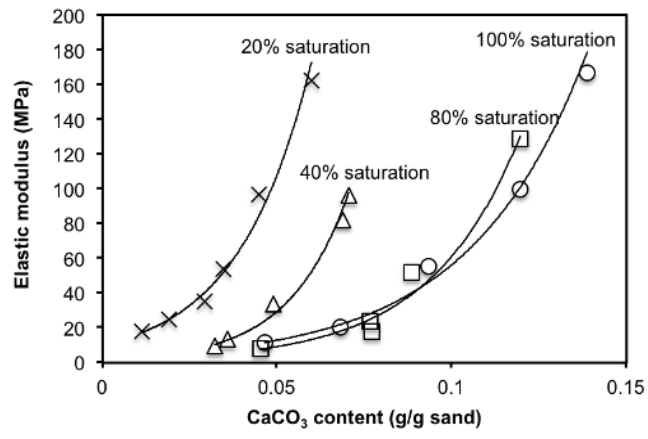


Fig. 4

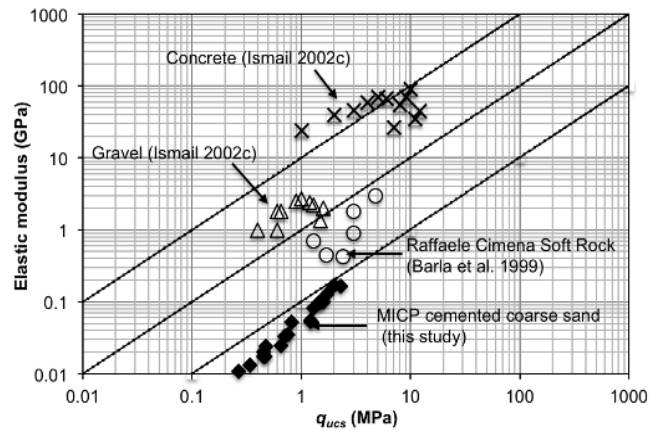


Fig. 5

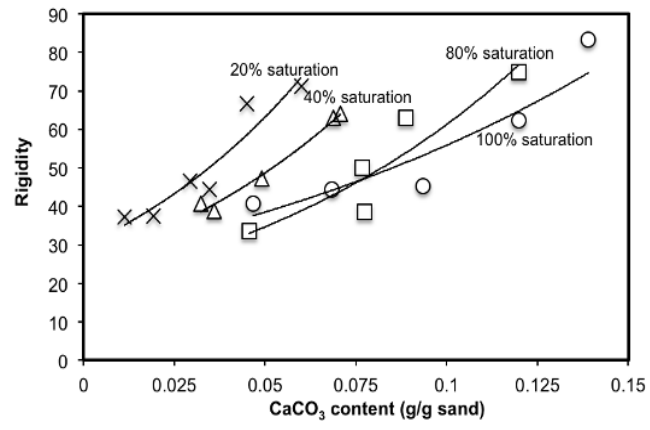


Fig. 6

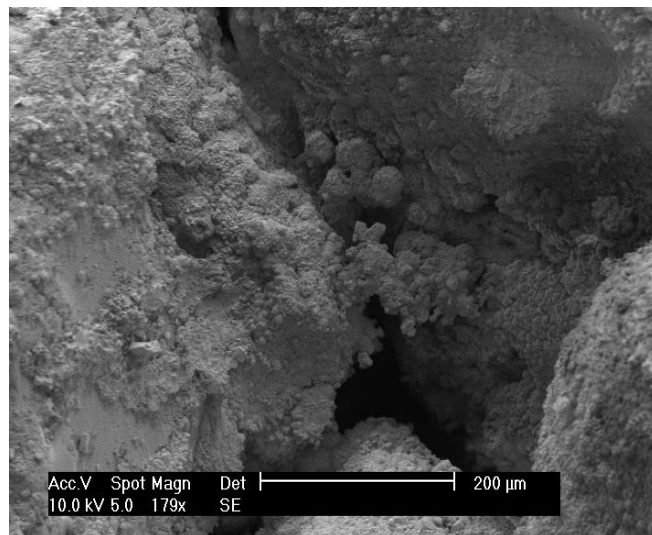
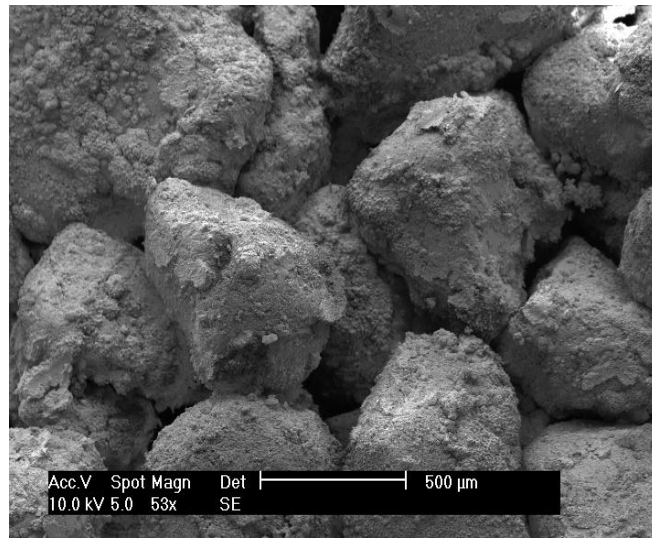


Fig. 7

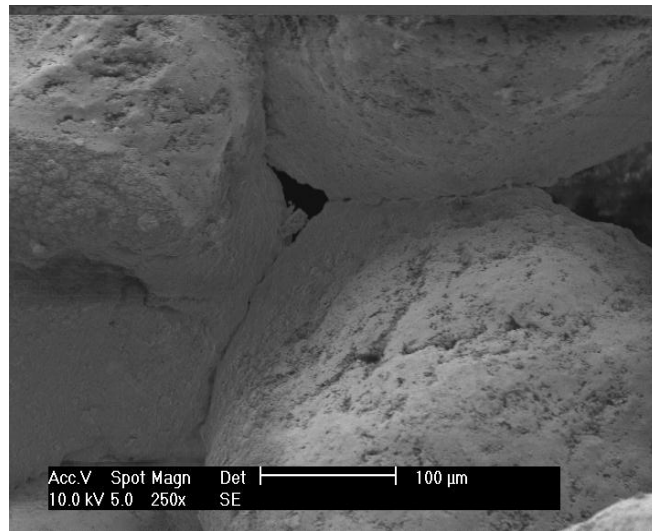
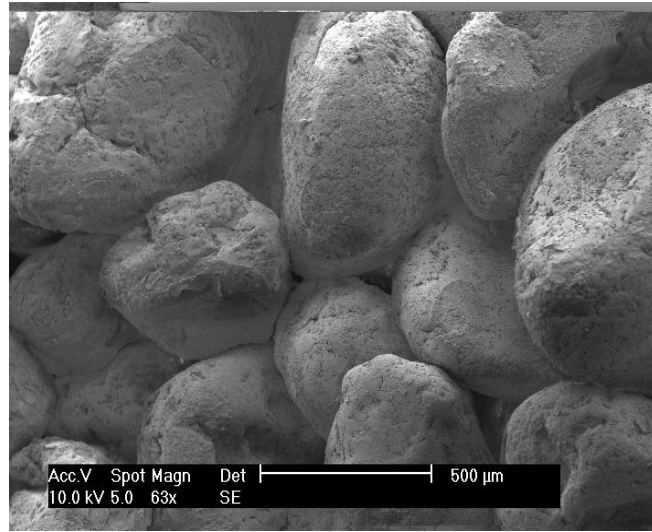


Fig. 8

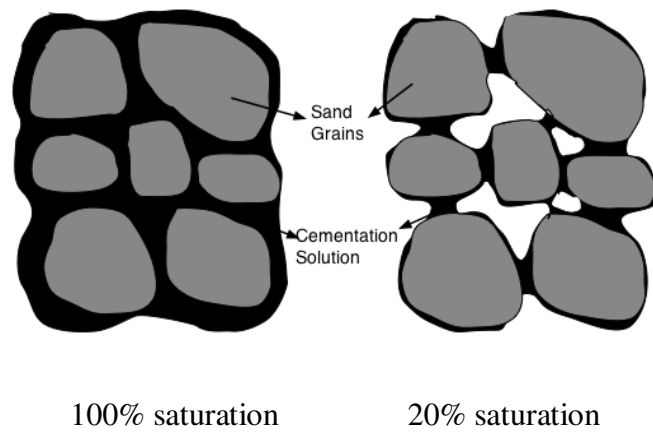


Fig. 9

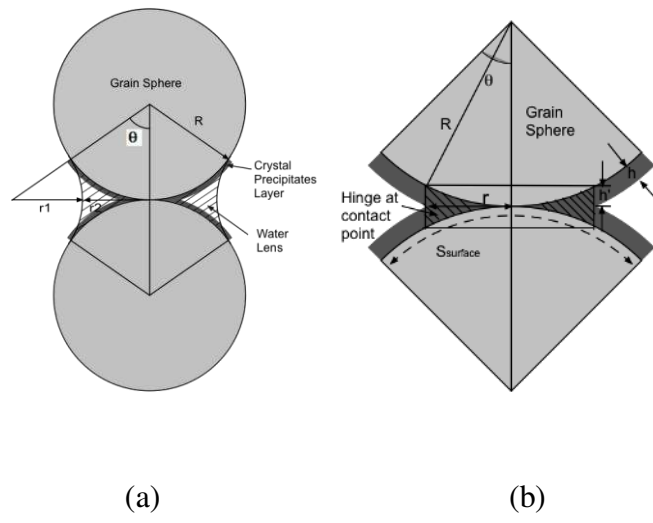


Fig. 10

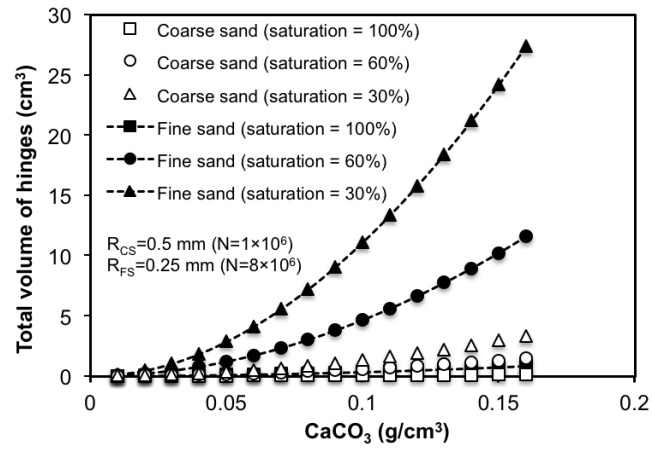


Fig. 11

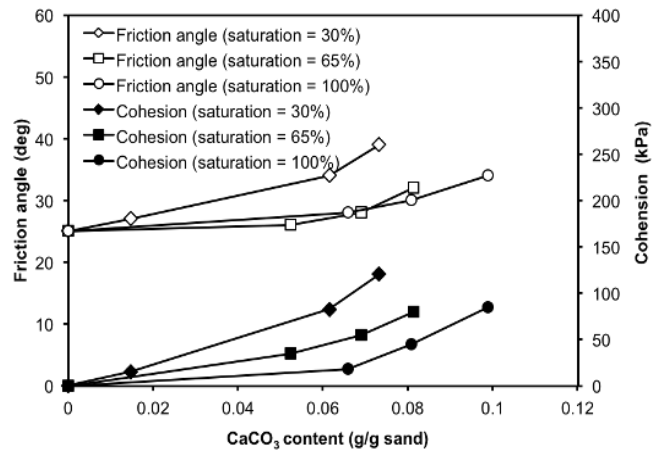


Fig. 12

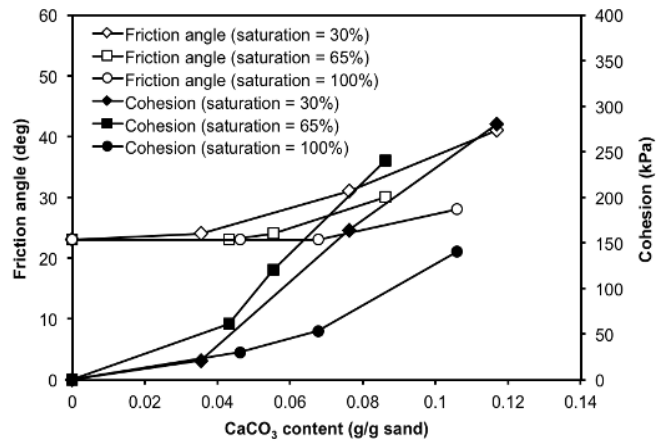


Fig. 13

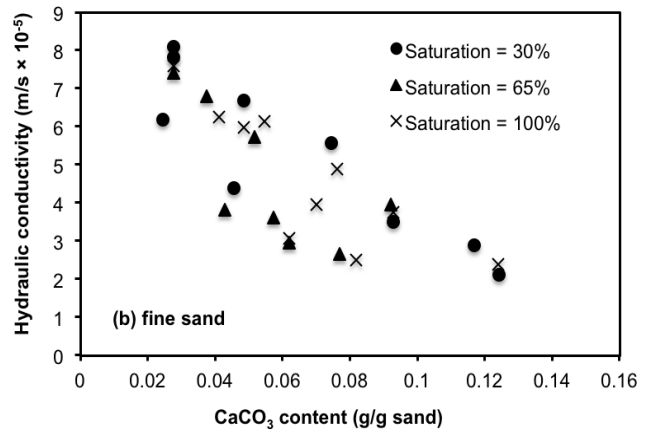
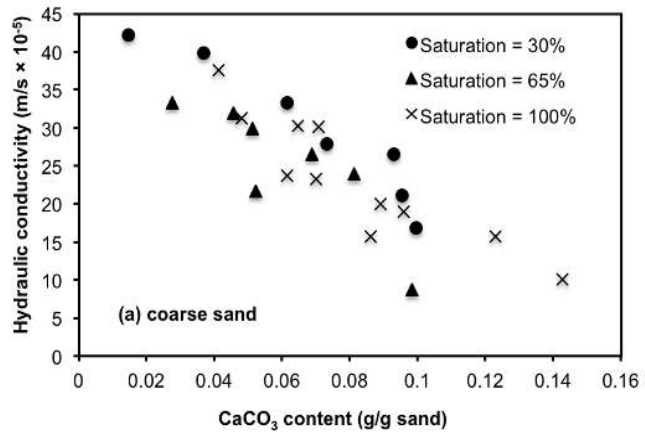


Fig. 14

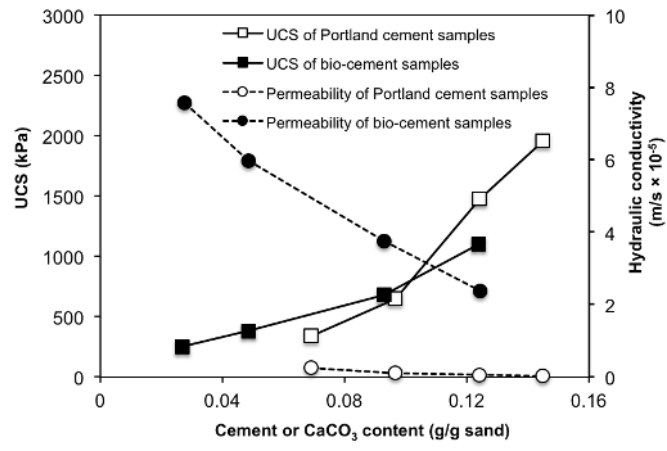


Fig. 15

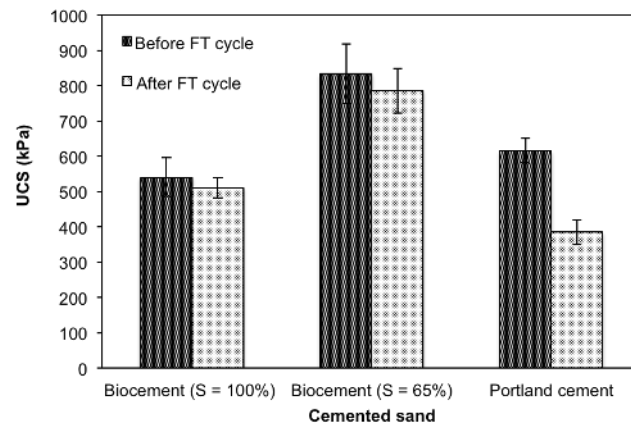


Fig. 16

